university of groningen

Improving the Flow Pattern in Pipes by Using Elbows as Flow Straighteners

How can the flow pattern after an elbow be improved by modifying the structure of the elbow in order to prevent vortices?

Sophie La Rondelle
S4520394
s.la.rondelle@student.rug.nl
Bachelor Research Project
WBCE901-15

Faculty of Science and Engineering
University of Groningen
The Netherlands
21 June 2023

Dr. Ir. P. D. Druetta
Asst. Prof. D. Parisi

Abstract

In this paper, four different flow straighteners inside the elbow part of a pipe were designed. The behaviour of a turbulent water flow through these flow straighteners in three different piping systems was simulated. The aim was to improve the flow pattern after an elbow by modifying the structure of the elbow. This paper documents the plots of the velocity streamlines, pressure distribution and vorticity field for the simulations that have been made to predict the behaviour of the flow. The research was performed by developing Computational Fluid Dynamic (CFD) simulations in COMSOL Multiphysics while employing the κ-ε model as the RANS turbulence model to analyse the turbulent flow. The mesh and geometry of the models were also created in COMSOL. The study focuses on the vorticity development and pressure distribution of the fluid through the systems. One of the main findings was that Disturbance Plate A, which contained a pipe in the center of the elbow with a diameter of 0.5·D and ten smaller pipes with diameter of 0.2·D around it, showed the best results in reducing the vortex formation in a short straight pipe run after the elbow. Furthermore, after analysing the experimental results for the pressure drop, the relation between the pressure drop and the surface area was found to be exponential. Finally, some recommendations were made to improve the accuracy of the results in the experiments.

Table of Contents

List of Figures

List of Tables

Nomenclature

Variables

ϵ	dissipation rate of turbulent kinetic energy $[m^2/s^3]$
η	dynamic viscosity $[Pa \cdot s]$
κ	turbulent kinetic energy $[J/kg]$
$\langle u_i \rangle$	mean velocity field of flow $[m/s]$
ν	kinematic viscosity $[m^2/s]$
$\overline{u'^2}$	time-average fluid velocity $[m/s]$
ρ	density of water $[kg/m^3]$
τ	turbulent stress tensor $[N/m^2]$
A	area $[m^2]$
F	scalar force potential $[N]$
f	arbitrary function $[-]$
f	body force $[N]$
n_i	outward-pointing unit normal of control volume $[-]$
$P(u)$	probability density function $[-]$
p	pressure $[Pa]$
$R_{ij}(u)$	Reynolds stress tensor $[N/m^2]$
S	surface of control volume $[m^2]$
S_{ij}	rate-of-strain tensor $[s^{-1}]$
t	time $[s]$
u_i'	fluctuating velocity field of flow $[m/s]$
u	random variable $[-]$
u_i	velocity field of flow $[m/s]$
V	(control) volume $[m^3]$
x	position of particle $[m]$

1 Introduction

Accurate measurement of the total volumetric flow rate through a piping system is one of the main challenges in monitoring the production behavior in industry. Pipe systems in industry rarely consist of straight sections solely [1], but rather consist of a combination of straight sections and disturbances in the form of elbows, tees and valves that distort the flow pattern. For upstream disturbances, a straight run piping of twenty five to forty pipe diameters is required to obtain a restored flow profile and for downstream disturbances a straight run of four to five pipe diameters is required [2]. Providing sufficient straight run piping to obtain a fully developed flow profile is not always possible in industry, therefore flow straighteners are used.

Several flow straighteners in straight pipes have been developed over the years to improve the measurement accuracy of the flow by reducing its disturbances [3], however the disturbances itself are not created in the straight pipe but in the elbow of the pipe. By designing a flow straightener inside the elbow, the swirl of the fluid in the elbow can be eliminated and a repeatable velocity profile can be created to restore the flow pattern at a shorter distance in the straight pipe [4]. The purpose of this work was to investigate the flow pattern of water inside three different piping system when four different flow straighteners are placed inside the elbows, using Computational Fluid Dynamics (CFD) models. The first system consisted of an upstream flow with one 90° elbow, the second system contained two 90° elbows located in-plane and the third systems contained two 90° elbows located out of plane relative to each other.

The behaviour of laminar and turbulent fluid flows can be described by the *Navier-Stokes equations*. The Navier-Stokes equations are named after the French physicist and engineer Claude-Louis Navier and the Irish physicist George Gabriel Stokes. The equations show how the density, temperature, pressure and velocity of a moving fluid are related via diffusion and convection [5]. The equations are derived from the Euler equations and are used to determine the velocity of a specific component of the flow at a particular position and time [6]. The effect of the viscosity of the fluid is neglected in the Euler equations, but this effect is taken into account in the Navier-Stokes equations, making the Navier-Stokes equations more complete to describe the behaviour of fluids. For non-Newtonian fluids, the relationship between the shear rate and the shear stress can be time dependent, which would make the Navier-Stokes equations not valid [7]. Water was chosen as fluid in this research paper, which is a Newtonian fluid, hence the Navier-Stokes equations can be applied to stimulate the flow of water. These equations cannot be solved analytically without making approximations and simplifications to the equations, but high-speed computers are capable of approximating the equations. CFD can be used as a numerical computation method to simulate many physical phenomena, including the velocity profile of a fluid through a piping system [6]. COMSOL Multiphysics is used as CFD software in this research paper.

This research paper aims to answer the following research question:

How can the flow pattern after an elbow be improved by modifying the structure of the elbow in order to prevent vortices?

Vortices or eddies are swirling fluid structures and reverse currents that are created in turbulent flows (*Reynolds number* > 4000). This results in a movement and direction of the fluid that deviates from the general flow of the fluid. As the velocity of the fluid flow increases, the number of eddies in the flow will also increase [8]. Turbulent flows contain large and small eddies, however small eddies are usually not described in the numerical simulations. The behaviour of turbulent flows therefore cannot be described accurately with the Navier-Stokes equations. An alternative approach for this is called the *Reynolds-averaged Navier Stokes (RANS) equations*, which predicts the average behaviour of turbulent flows [9].

2 Model Description

2.1 Physical Model

An elbow in a piping system creates resistance that is translated into a pressure drop. The shape and curve radius of this elbow make a large difference in the size of the resistance that is created. In this study, the radius of the curve, the diameter of the pipe and the inlet and outlet pipe length are kept constant. The system is defined to be isothermal with a constant temperature of 363.15 K. The independent constants can be found in Table 1 [10].

Table 1: Independent Constants.

Name	Value	Description
D	0.0355 m	Pipe diameter
L_{in}	0.07 m	Inlet length
L_{out}	0.35 m	Outlet length
R_c	0.05 m	Coil radius
ρ_{fluid}	965.35 kg/m^3	Density of fluid
μ_{fluid}	3.14×10^{-4} Pa·s	Dynamic viscosity
u_{avg}	5 m/s	Average velocity
T	363.15 K	Temperature of system

2.1.1 Elbow Structures and Benchmark Cases

The constants described in Table 1 are used to create three-dimensional benchmark models to validate the found results. The geometries for the three different benchmark cases that were created for the purpose of this study are depicted in Figure 1. The first system contains an upstream flow with one single 90° elbow (Figure 1a), the second system contains two 90° elbows that are located in-plane relative to each other (Figure 1b) and the third system contains two 90° elbows out of plane (Figure 1c). For the model with one elbow and the model with two elbows in-plane, only half of the pipe was modelled since models that are in-plane are symmetrical. For the model that contained two elbows out of plane, the entire pipe had to be modelled.

(a) One elbow. (b) Two elbows in-plane. (c) Two elbows out of plane.

Figure 1: Three different benchmark cases.

A total of four different elbow structures was designed to improve the flow pattern in the piping systems. The goal was to create a flow pattern of water through the systems for which the velocity profile would not be distorted after the elbow. In industry, flow straighteners in straight pipelines for turbulent flow contain tubes or disturbance plates [3], therefore two different types of disturbance plates were designed in this study.

The first flow straightener that was designed was a fin type flow straightener. This flow straightener consisted of eight blades that all come together at the centre of the pipe. Each blade makes an angle of 45 degrees relative to blades next to it. The blades are only placed in the part of the pipe that contains the elbow, not in the straight pipelines. All the blades were defined as interior walls in COMSOL. For the second flow straightener, a disturbance plate with pipes of different sizes was designed (this flow straightener will be referred to as Disturbance Plate A). The centre of the elbow contained a smaller pipe with a diameter equal to 0.5·D. Around this centre pipe, a total of ten smaller pipes with a diameter of 0.2·D were placed, each with equal distance to the wall, the centre pipe and the other small pipes. The third flow straightener contained sixteen equally sized pipes in a disturbance plate throughout the entire elbow (Disturbance Plate B). The diameter of one single pipe is equal to 0.15·D. The vertical and horizontal distance between two pipes is 0.04·D and the pipes are located in an array with three pipes in the top and bottom rows and five pipes in the middle rows. The fourth and final flow straightener that was designed contained a netting structure. This netting structure was designed by creating three parallel horizontal and three parallel vertical interior walls that were separated by a distance of 0.25·D. All four different elbow structures are depicted in Figure 2.

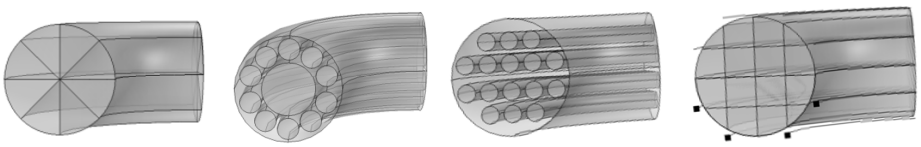

Figure 2: Four different models for flow straighteners in elbows.

2.1.2 Meshing

After the geometry for all the models had been designed, a meshing had to be built before the simulations with the different flow straighteners could be run. The mesh of a model affects the accuracy by which a model is solved [11]. The size, number of elements and the element quality of the mesh can be customized in COMSOL. Ideally, the mesh would be extremely dense, but since solving an extremely dense mesh takes a lot of time, compromises had to be made. In COMSOL, the mesh can be generated automatically by using the physics-controlled mesh as a sequence type in which the element size can be varied from *extremely fine* to *extremely coarse*. The mesh can be customized with the user-controlled mesh. The settings for the global size, corner refinement and boundary layers of the mesh can be adjusted for this type of mesh.

A user-controlled mesh was applied to all the models in this study. For the models with one elbow and two elbows in-plane, a custom element size for the mesh was generated. The parameters for this custom mesh are shown in Table 2. These parameters were also used to generate a mesh for the benchmark model and the fin type model for the piping system with two elbows out of plane. For the other three models that contained two elbows out of plane, it quickly became evident that simulating these models with the same mesh would take days. Hence, a predefined mesh with a global element size of *normal* was rendered to solve these models. The cell arrangement that was used for the meshing in this study was free triangular

and rectangular. A close-up of the element distribution over a part of the elbow in the meshing is shown in Figure 3.

Table 2: Meshing Parameters

Name	Value
Maximum element size	D/20 m
Minimum element size	8.03×10^{-5} m
Maximum element growth rate	1.08
Curvature factor	0.3
Resolution of narrow regions	0.95

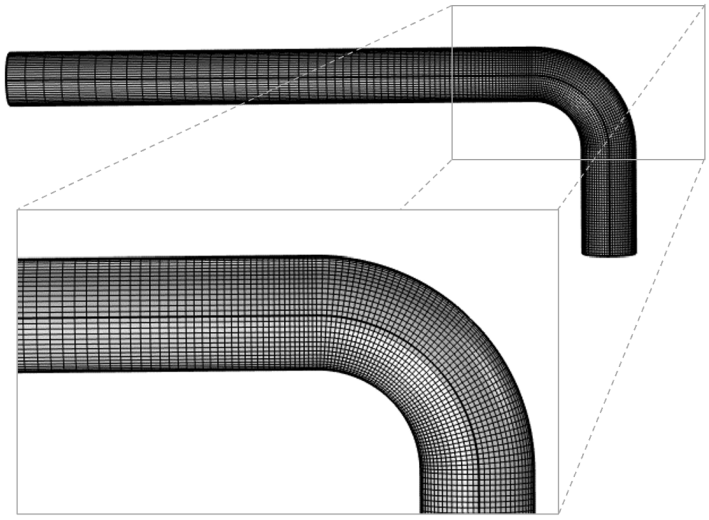

Figure 3: Element distribution of the mesh.

2.1.3 Turbulence Model

A numerical method is used for the calculation of turbulent flows. COMSOL provides eight different Reynolds-Averaged Navier-Stokes (RANS) models to model turbulent flow in the CFD Module. These models are used to predict turbulent flow. Laminar fluid flow is modelled by means of the Navier-Stokes equations that consist of multiple non-linear and time-independent equations. For turbulent flow, the velocity field varies with times, making the Navier-Stokes equations not accurate to predict the behaviour of turbulent flow. Hence, time-dependent Navier-Stokes equations in the form of the RANS equations are used to predict turbulent flow. In the RANS equations, the average behaviour of the flow is used to describe the motion of turbulent flows.

The RANS model that is used in this thesis is the nonlinear κ-ϵ model, which solves the turbulent kinetic energy κ and the dissipation rate of turbulent kinetic energy ϵ. The model is developed by Launder and Spalding and it is based on computational fluid dynamics. It relatively accurately calculates the flow through pipes with elbows for low Reynolds numbers and it is known for its good convergence rate [12].

The turbulent kinetic energy per unit mass κ is described by

$$\kappa = \frac{1}{2}\overline{u'^2} \tag{1}$$

where $\overline{u'^2}$ is the time-average of the fluid velocity.

2.2 Mathematical Model

2.2.1 Navier-Stokes and Reynolds-Averaged Navier-Stokes equations

The Navier-Stokes equations for incompressible Newtonian fluids such as water at constant temperature are described by

$$\frac{\partial u_i}{\partial x_i} = 0, \tag{2a}$$

$$\frac{\partial u_i}{\partial t} + \frac{\partial}{\partial x_j}(u_i u_j) = -\frac{1}{\rho}\frac{\partial p}{\partial x_i} + 2\nu\frac{\partial S_{ij}(u)}{\partial x_j} + \frac{1}{\rho}f_i. \tag{2b}$$

As described earlier, the Reynolds-Averaged Navier-Stokes equations predict the behaviour of turbulent flow by obtaining information about the average behaviour of turbulent flows. With the publication of *Papers on Mechanical and Physical Subjects*, *Vol. 3* by Osborn Reynolds in 1895, the term *Reynolds decomposition* was introduced [13]. This term comprises the decomposition of the velocity field of flows u_i,

$$u_i = \langle u_i \rangle + u_i', \tag{3}$$

into the mean velocity $\langle u_i \rangle$ and the relative velocity u_i'. The mean velocity can be determined with a statistical averaging method that is known as *Reynolds averaging* [14]. The Reynolds average can be expressed as

$$\langle u \rangle = \int_{u=-\infty}^{\infty} uP(u)\,du. \tag{4}$$

The *probability density fuction* $P(u)$ has to be non-negative and normalized for Eq. 3 to be valid [14]. The normalization of the probability density function is described by

$$\int_{u=-\infty}^{\infty} P(u)\,du = 1. \tag{5}$$

A more general way to describe the Reynolds average is defined through the equation

$$\langle f(u) \rangle = \int_{u=-\infty}^{\infty} f(u)P(u)\,du. \tag{6}$$

in which $f(u)$ can be any arbitrary function.

To obtain the Reynolds-Averaged Navier-Stokes equations, the Reynolds averaging procedure described by Eq. 4 to 6 are applied to the Navier-Stokes equations (Eq. 2a and 2b). The RANS equations can be written as

$$\frac{\partial \langle u_i \rangle}{\partial x_i} = 0, \tag{7a}$$

$$\frac{\partial \langle u_i \rangle}{\partial t} + \frac{\partial}{\partial x_j}(\langle u_i \rangle \langle u_j \rangle) = -\frac{1}{\rho}\frac{\partial \langle p \rangle}{\partial x_i} + 2\nu \frac{\partial S_{ij}(\langle u \rangle)}{\partial x_j} + \frac{\partial R_{ij}(u)}{\partial x_j}. \tag{7b}$$

In these Reynolds-Averaged Navier-Stokes equations, $\langle u_i \rangle$ describes the average velocity and $\langle p \rangle$ represents the pressure fields. $S_{ij}(\langle u \rangle)$ represents the average rate-of-strain tensor that is described by

$$S_{ij}(\langle u \rangle = \frac{1}{2}\left(\frac{\partial \langle u_i \rangle}{\partial x_j} + \frac{\partial \langle u_j \rangle}{\partial x_i}\right). \tag{8}$$

It is not possible to express the *Reynolds stresses* $R_{ij}(u)$ in terms of the mean velocity $\langle u_i \rangle$. This results in more unknowns than equations in Eq. 7, making the RANS equations unsolvable. To simulate turbulent flows in COMSOL, solutions for the average velocity $\langle u_i \rangle$ and pressure fields $\langle p \rangle$ are approximated by using the Reynolds stresses.

2.2.2 Conservation of Mass

In 1789, Antoine Lavoisier formulated the Law of Conservation of Mass that stated that mass cannot be created nor destroyed in a closed system [15]. For a fluid with a density ρ that flows through a pipe with a boundary surface S of a fixed controlled volume V, this results in a rate of change of mass flow in the controlled volume of

$$\frac{d}{dt}\int_V \rho \, dV = \int_V \frac{\partial \rho}{\partial t} \, dV = -\oint_S \rho u_i n_i \, dS. \tag{9}$$

u_i is a velocity field vector of the flow that contains components in all three spatial directions in the Cartesian coordinate system. The normal unit that is pointing outwards of the control volume is described by n_i. The final term of Eq. 9 describes the origin for the change in mass flow that the control volume S contains. The mass flow is transported through the surface S by the velocity u_i, hence Eq. 9 describes the conservation of mass.

For fluids with a so-called smooth density (i.e. no unexpected results), Eq. 9 can be rewritten as

$$\frac{d}{dt}\int_V \rho \, dV = \int_V \frac{\partial \rho}{\partial t} \, dV = -\int_V \frac{\partial}{\partial x_i}(\rho u_i) \, dV. \tag{10}$$

For the pipe systems in this study, the control volume V is chosen arbitrarily. Therefore, the conservation of mass is equal to

$$\frac{\partial u_i}{\partial t} + \frac{\partial}{\partial x_j}(u_i u_j) = 0. \tag{11}$$

Equation 11 is the *differential formulation* that describes the density as a function of position in an inertial reference frame [14]. For an arbitrarily volume, the differential formulation is equal to the integral formulation.

Since water is a Newtonian fluid, the density ρ of water is constant over time and uniform in space. Consequently, the conservation of mass in Eq. 9 can be reduced to

$$\frac{\partial u_i}{\partial x_i} = 0, \tag{12}$$

which is the *incompressibility condition* of the flow. The mass in a system is conserved if the velocity field or incompressible flow does not diverge. An incompressible fluid like water has a incompressible flow as a consequence of the constant density of water. The rate of change between the mass that enters and leaves the system is zero, meaning that the local volume expansion rate is also zero.

2.2.3 Rheology

The flow of liquids is described with rheology. The viscosity of a fluid is a term that is used to express how resistant a fluid is to flow. As explained before, water is a Newtonian fluid. The strain rate, which is the rate of change of deformation of the fluid over time, is linearly related to the viscous stresses of the fluid for Newtonian fluids. These viscous stresses are directly proportional to the rate of change of the velocity vector of the fluid [16].

The relation between the viscous stresses and the strain rate can best be described by the $two - plate\ model$. This model consists of two plate with a fluid that is placed between those plates. One of the plates is stationary and not moving, while the other plate shifts very slowly. The shift of this plate causes the fluid to experience a shear stress that is parallel to the surface of the plate. The shear stress is defined as the force that is applied to shift the plate divided by the area of the plate $\tau = \frac{F}{A}$ [17]. The shear rate $\frac{dv}{dr}$ can also be calculated with this two-plate model by introducing the dynamic viscosity η which results in

$$\tau = \frac{F}{A} = \eta \frac{dv}{dr}. \tag{13}$$

2.3 Boundary Conditions

Before the Reynolds-Averaged Navier-Stokes equations can be solved, boundary conditions have to be specified. In COMSOL, a boundary system can be specified in terms of a vector system to create boundary conditions in normal or tangential directions on the boundary that is not aligned with the Cartesian coordinate system. In this study, 3D models are simulated in which the coordinate system is defined by (t_1, t_2, $\mathbf{n}$). The vectors t_1 and t_2 represent the tangential directions while $\mathbf{n}$ reflects the normal direction. The cross product between the vector $\mathbf{n}$ and the vector t_1 is described by t_2.

A boundary condition that can be used to solve the incompressible Navier-Stokes equation is to set the velocity field to zero at the solid boundaries. This results in no tangential velocity at the solid boundaries ($no - slip\ condition$). A second condition called the *impermeability condition* is used to specify the boundary conditions in which no normal velocity is allowed at solid boundaries [14].

The first boundary of the fluid domain is the symmetry plane at $z = 0$. At this border, the change in velocity is equal to zero for all the flow variables. The second boundary is the inlet of the pipe ($x = 0$). If the axial velocity would be equal to the average velocity, the no-slip condition would not be satisfied, which is not realistic. Therefore, a non-uniform axial velocity profile should be enumerated. The outlet of the system is the third boundary. One of the requirements is that gauge static pressure should be reached at the outlet of the system. The walls are the fourth and final boundaries of in the systems. The no-slip condition results in a velocity of zero for all three Cartesian coordinates at the wall [18]. Lastly, the walls of the pipes are defined to be smooth.

3 Results and Discussion

In the presentation of the results, the focus will be on the vorticity development and the pressure distribution. Furthermore, variables such as the pressure drop and velocity streamlines will be analysed. Fifteen simulations were carried out in COMSOL; three benchmark models and twelve models with various flow straighteners. The three different benchmark models are used to validate various aspects of the numerical method, such as the pressure drop and the vortex generation. The vortex development was measured at multiple points in the piping system. The total length of the horizontal outlet pipe was 0.4 m (radius of elbow was 0.05 m and outlet length of pipe was 0.35 m). Two cut planes in the horizontal pipe were created, the first plane at a distance of 0.1 m (0.05 m after the elbow) and the second plane at a distance of 0.2 m (0.15 m after the elbow). Subsequently, the values and graphs for the benchmark cases are analysed and compared to the values and graphs for the modelled flow straighteners to see if the flow pattern of the fluid is restored with the help of flow straighteners inside the elbows.

3.1 Pressure Distribution

The pressure distribution on the symmetry surface of the inlet of the pipe system is uniform. The elbow has a significant effect on the pressure in the system, as can be seen in Figure 4. The pressure distribution on the symmetry plane relative to the atmospheric pressure illustrates the higher pressure region inside the elbow part that is generated by the curvature and the centrifugal force of the pipe. The pressure gradually decreases towards the inner wall of the bend. The pressure gradient inside the pipe contributes to the high velocity at the outer curve after the elbow, which is shown in Figure 7a.

Furthermore, it can be observed that the pressure at the outlet of the system is lower than the pressure at the inlet of the system. This is the result of frictional head loss of the flow along the pipe wall due to the viscosity of molecules. The pressure distributions for the other benchmark cases are depicted in Figure 5 and 6. Figure 5 shows the pressure distribution for the benchmark model with two elbows out of plane, while Figure 6 shows the pressure distribution for the two elbows out of plane. Both figures clearly show that the pressure of the inlet stream of the systems is higher than the pressure of the outlet systems. The pressure on the outside of the elbow is higher for both models than on the inside of the elbow, which was also observed for the benchmark case with one elbow.

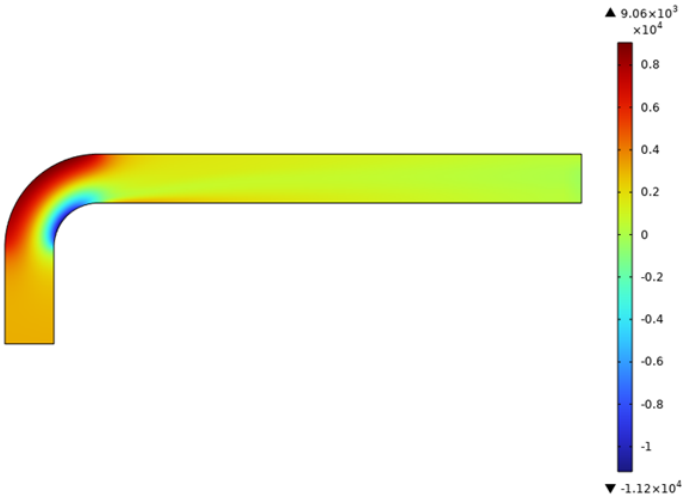

Figure 4: Pressure distribution on symmetry plane over pipe in system with one elbow.

Figure 5: Pressure distribution over pipe in system with two elbows in-plane.

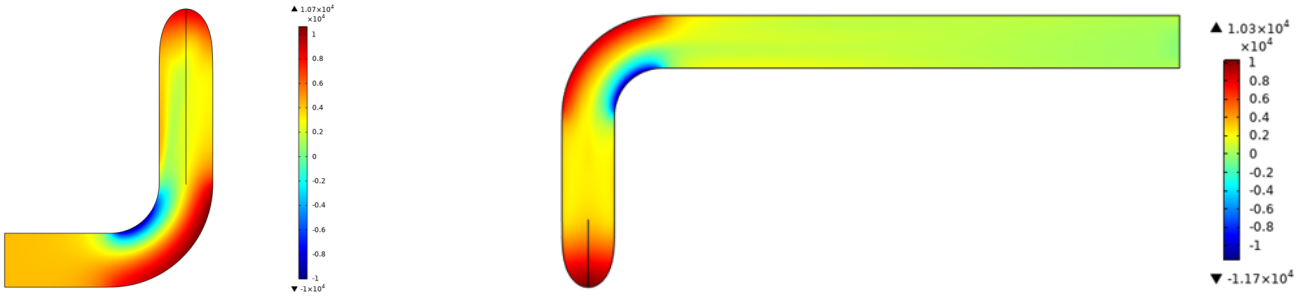

(a) Inlet of System. (b) Outlet of System.

Figure 6: Pressure distribution of pipe in system with two elbows out of plane.

3.2 Vorticity Field for Piping System with One Elbow

3.2.1 Benchmark Case with Velocity Streamlines

The velocity streamlines for the benchmark case with one elbow are depicted in Figure 7a. The contour of the velocity streamline plot shows a fully developed turbulent flow at the inlet op the pipe. Here, the fluid at the wall of the pipe has a velocity of zero as a result of friction with the wall. The velocity of the flow gradually increases to a maximum value of 6.5 m/s at the centre of the pipe. It is observed that the velocity streamlines are not parallel to each other inside the elbow part. The curved shape of an elbow actuates centrifugal forces on the fluid inside the pipe that influence the direction of motion of the fluid. This results in a flow separation in which the velocity towards the inside of the elbow is higher than the velocity towards the outside of the elbow. The fluid is moved towards the outside of the elbow due to the velocity gradient that is caused by the centrifugal forces, which results in vortices. At the end of the pipe in Figure 7a, the velocity streamline pattern is still distorted, meaning that the flow is not steady. The vorticity field (y-component) at the end of the elbow in Figure 7b shows that vortices are created at the inside of the elbow relative to the stream before the elbow. The goal of the flow straighteners is to reduce the size of the vortices that are created to restore the velocity streamline pattern before the end of the pipeline in this system.

After the bend, two vortices are formed that are counter-rotating. Theses vortices are caused by the centripetal force. For fluids flowing through a curved pipe, the Dean number is used as an additional dimensionless number to describe the flow pattern. The Dean number describes how the flow is influenced by the longitudinal and transverse curvature of a bend [1]. The force that makes a fluid follow the curve of a pipe is called the centripetal force. The direction of this force is perpendicular to the direction of the fluid and points towards the centre of the curve of a pipe. This force was described as “a force by which bodies are drawn or impelled, or in any way tend, towards a point as to the centre” by Isaac Newton [19]. The direction of motion of the fluid is influenced by the centripetal forces in the curve due to the formation of a pressure gradient. This results in a lower velocity of the fluid close to the wall compared to the velocity in the centre of the pipe. The fluid close to the centre of the curve is drawn towards the wall of the curve while the fluid near the wall returns to the centre of the curve. This motion is described by Dean vortices [20].

Since one of the vortexes is located on the other side of the symmetry plane, only one of the vortices is visible in Figure 7a.

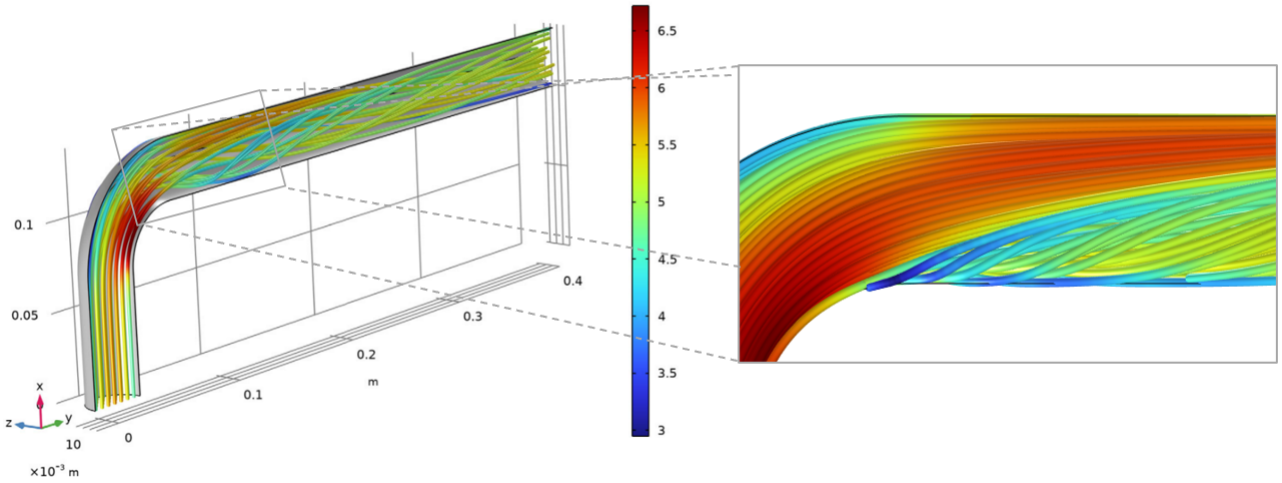

(a) Velocity Streamlines.

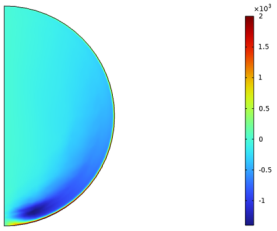

(b) Vorticity field.

Figure 7: Velocity streamlines and vorticity field for one elbow benchmark model.

3.2.2 Fin Type Flow Straightener

For the vorticity field study of the fin type flow straightener, multiple cut planes in the model were created to compare the vorticity development at multiple points in the pipe. The vorticity field contour plots at five different stages in the model are shown in Figure 8. Figure 8a depicts the vorticity field at the start of the elbow. The red colour indicates that no vortices are formed inside the straight inlet pipe run. At the 90-degree outlet of the elbow, big vortices are formed close to the interior walls of the flow straightener and at the wall of the pipe, which can be seen in Figure 8b. From Figure 8c it can be concluded that the vortices at distance of 0.05 m after the elbow have shifted from the interior walls to the outside wall of the pipe. In the center of the pipe, the magnitude of the vortices that are present lies between 0 and 100 $\frac{1}{s}$, while the magnitude of the vortices around the wall of the pipe is close to 300 $\frac{1}{s}$. The vortices in Figure 8d have a magnitude that varies between 0 and 100 $\frac{1}{s}$. When comparing the size of the vortices formed in the fin type flow straightener to the vortices in the benchmark model, it can be concluded that the fin type flow straightener reduces the vorticity field in the y-direction with about 75 percent after a straight run of 0.2 m compared to the benchmark case. The vorticity contour plots with their colour legends can be seen in Appendix A.

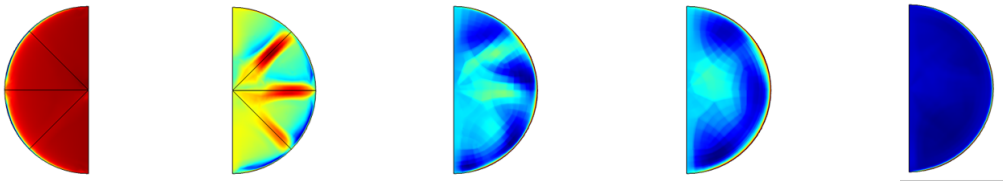

(a) Start of Elbow. (b) End of Elbow. (c) L = 0.1 m. (d) L = 0.2 m. (e) End of Pipe.

Figure 8: Vorticity field for fin type flow straightener.

3.2.3 Disturbance Plate Flow Straightener

The vorticity field contour plots for the two disturbance plate flow straighteners are depicted in Figure 9 and 10. The colour pattern of the vorticity field for both disturbance plates at a distance of 0.05 m after the elbow is significantly more even than the colour patterns for the benchmark case and the fin type flow straightener. Also the magnitude for the biggest vortices for Disturbance Plate A is about three times smaller than the magnitude for the fin type flow straightener. For Disturbance Plate B, the vorticity magnitude is of similar order to that of the fin type flow straightener. By looking at the vorticity field, it can be concluded that the disturbance plate flow straighteners prevent the formation of eddies more successfully than the fin type flow straightener does at a distance of 0.05 m after the elbow.

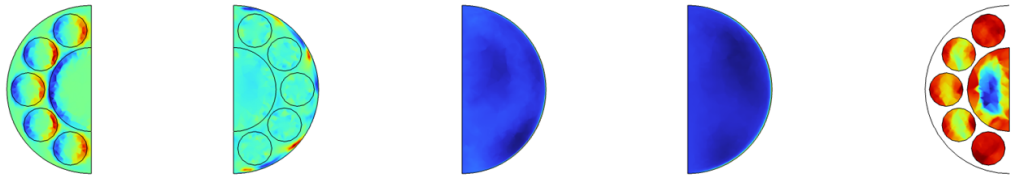

(a) Start of Elbow. (b) End of Elbow. (c) L = 0.1 m. (d) L = 0.2 m. (e) Halfway Elbow.

Figure 9: Vorticity field for disturbance plate A flow straightener.

Note that the magnitude for vorticity field in Figure 9c-d is about five times smaller than the magnitude in Figure 10c-d (see Appendix A). This has to be taken into account when comparing the vorticity generation for both models.

(a) Start of Elbow. (b) End of Elbow. (c) L = 0.1 m. (d) L = 0.2 m. (e) Halfway Elbow.

Figure 10: Vorticity field for disturbance plate B flow straightener.

3.2.4 Netting Structure Flow Straightener

Figure 11 illustrates the contour plots of the netting structure flow straightener at all five stages in the piping system. The formation of vortices was not prevented with this flow straightener. In the outlet of the system, vortices are still present in the fluid. The colour of the plot in

Figure 11e ranges from red to dark blue, which indicates that vortices of multiple sizes are still present. For the benchmark model, there were almost no vortices present after a straight pipe run of 0.35 m. Hence, the benchmark model performs better in preventing the formation of vortices than the netting structure flow straightener.

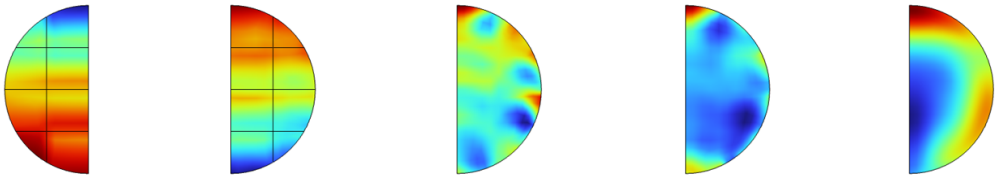

(a) Start of Elbow. (b) End of Elbow. (c) L = 0.1 m. (d) L = 0.2 m. (e) End of Pipe.

Figure 11: Vorticity field for netting structure flow straightener.

3.3 Vorticity Field for Pipe Systems with Two Elbows

The vorticity contour plots for the models with two elbows in and out of plane are given in Appendix B and C. Note that some vorticity contour plots in Appendix C do not have a perfect circular shape, which is the result of using a less detailed meshing in the simulations. Figure 12 shows the velocity streamlines for both models.

The benchmark cases show similar results as the benchmark case with one elbow. Vortices are formed in the elbows of the pipe systems and the vortices remain present in most of the straight pipe run. At the outlet of the systems, after a straight pipe run of four times the diameter, nearly all the vortices have disappeared and the flow pattern is sufficiently restored to measure a constant velocity pattern.

The fin type flow straightener shows a increased formation of vortices for the system with two elbows out of plane. For the two elbows in plane, this flow straightener does show a decrease in vortex formation, but after the entire straight run vortices are still present in the system.

The Disturbance Plate A clearly performs better than Disturbance Plate B for both systems. This was also the case in the system with one elbow. At the end of the straight pipe run, almost no vortices are present in the system for both disturbance plates. After a straight pipe run with a length of one diameter, the largest vortices present in the system have similar size as the vortices present at the end of the system for the benchmark model for Disturbance Plate B. Therefore, the model with Disturbance Plate A shows a significant improvement to prevent vortices in the system.

The netting structure flow straightener also shows an improvement for the system with two elbows out of plane. Interesting to notice is that the magnitude of the vortices at the end of the system are bigger than the magnitude at earlier points in the straight pipe run. No clear explanation for this result was found, except that the meshing of this piping system was not as detailed as for the other piping systems. For the system with two elbows in plane, the magnitude of the vortices decreased throughout the straight pipe run. This result is more in accordance with the expected results.

By looking at the vorticity plots solely, the Disturbance Plate A shows the biggest improvement in the reduction of vortices at the length of 0.05 m after the elbow.

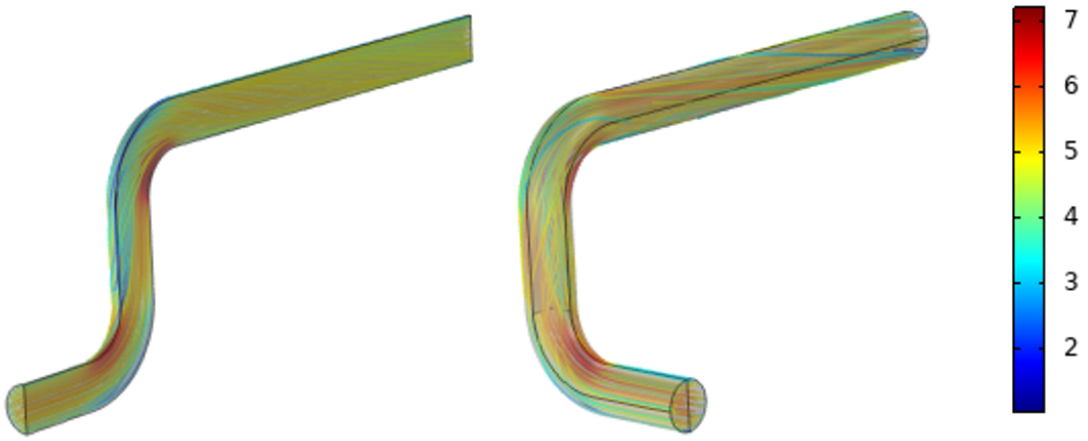

Figure 12: Velocity streamlines for benchmark models with two elbows in- and out of plane.

3.4 Pressure Drop over Elbows

Since the fluid is streaming upwards in the systems in this study, the pressure of the inlet stream will be higher than the pressure of the outlet stream. The pressure drop of the water flow over the elbows is shown in Table 3. For the benchmark cases, the pressure drop over the first elbow is similar for all three piping systems. The pressure drop over the second elbow is also similar for the systems with two elbows, but lower than the pressure drop in the first elbow. Generally, the pressure drop over a 90-degree elbow bend is equivalent to the pressure drop over a straight pipe with a length of 30 - 50 pipe diameters [21]. Since the inlet pressure of the second elbow is lower than the inlet pressure of the first elbow, the loss of pressure is also smaller. This relationship is also found for the fin type flow straightener and the netting structure flow straightener. The pressure drop over the elbows for the disturbance plate is significantly bigger than the pressure drop for the other models. This has to do with the surface area inside these elbows. For disturbance plate A, the surface area inside the elbow is 65 % of the surface area without a flow straightener. For disturbance plate B, the surface is even more decreased to 35 %. The pressure and surface area are inversely proportional. Hence, the pressure drop increases exponentially when the surface area of the pipe decreases. In Appendix D, a plot for the relative surface area against the pressure drop can be found.

Table 3: Pressure Drop over Elbows in Pascal.

Flow Straightener	One Elbow	Elbow 1 in-plane	Elbow 2 in-plane	Elbow 1 out of plane	Elbow 2 out of plane
Benchmark Case	842.8	808.6	517.6	820.4	465.5
Fin Type	1035.5	748.9	657.5	1076.3	905.2
Disturbance Plate A	30885	22708	23271	44555	44952
Disturbance Plate B	158287	156123	162578	209750	320182
Netting Structure	1244	1118	980.5	1821	878.8

3.5 Discussion

The κ-ϵ model was the only turbulence RANS model that was used to model turbulent flow in a pipe. It is recommended to also examine other simulation models such as the LES (Large-Eddy Simulation) or the ReNormalization Group (RNG) theory to validate the results. The RNG model contains more terms than the κ-ϵ model and therefore computes turbulent flows with swirl more accurately. Both the RNG and κ-ϵ model predict the turbulent flow without computing instantaneous fluctuations u_i'. The LES method is a more sophisticated method that simulates the largest eddies but also takes the effects of the smaller eddies into account [18]. However, simulations that use the LES method do take on much more time than simulations with the κ-ϵ model.

A simplification that was made in creating the models is associated with the mesh. To evaluate whether increasing the mesh resolution would significantly changes the simulated results, one would have to simulate the same models using a progressively finer mesh and increasing the number elements of the mesh. The run time for these models will increase drastically, which can be expensive.

Also, the systems were defined to be isothermal. Gravity-related effects such as buoyancy were therefore not taken into consideration. Since buoyancy was neglected, the flow was considered to be symmetric for the system with one elbow and the system with two elbows in-plane, but the buoyancy cannot be neglected when modelling elbow flow straighteners for industrial purposes.

4 Conclusion

Four different elbow flow straighteners were modelled in COMSOL Multiphysics while using CFD simulations. The goal was to define how the flow pattern after an elbow can be improved by modifying the structure of the elbow in order to prevent vortices. The first conclusion that has been drawn is that the above simulations with flow straighteners show a clear improvement of the flow pattern over the standard elbows without flow straighteners that are used in industry nowadays. By looking at the pressure drop, vorticity field and magnitude and the pressure distribution, it was concluded that Disturbance Plate A, which contained one big pipe at the center (diameter = 0.5·D) and ten smaller pipes around it (diameter = 0.2·D), showed the most promising results. The κ-ϵ model was used as RANS model to model the turbulent flow, but one would have to examine other CFD models to confidently conclude that the Disturbance Plate A flow straightener shows the best improvement in reducing the formation of vortices. The pressure drop over the elbows for this disturbance plate was significantly bigger than the pressure drop for the flow straighteners with a constant surface area throughout the system. On the other hand, the pressure drop for this disturbance plate was lower than for Disturbance Plate B, which had a surface area of about 50% compared to Disturbance plate A. The simulation's general results for the pressure drop over the elbow is in reasonable agreement with experimental data. The pressure drop increases exponentially when the surface area of the bend is decreased. Also the pressure distribution over the system is in accordance with the expected results as a result of the centripetal force in the elbow.

5 References

[1] S. Wegt, R. Maduta, J. Kissing, J. Hussong, and S. Jakirlić. Les-based vortical flow characterization in a 90°-turned pipe bend. *Computers and Fluids*, 240:105418, 5 2022. ISSN 0045-7930. doi: 10.1016/J.COMPFLUID.2022.105418.

[2] J. C. R. Hunt, A. A. Wray, and P. Moin. Eddies, streams, and convergence zones in turbulent flows. *Studying Turbulence Using Numerical Simulation Databases*, 12 1988.

[3] Blogger. How a flow conditioner works - flow conditioning basics, 2022.

[4] A. Erdal. A numerical investigation of different parameters that affect the performance of a flow conditioner. *Flow Measurement and Instrumentation*, 8:93–102, 6 1997. ISSN 0955-5986. doi: 10.1016/S0955-5986(97)00032-0.

[5] Doug McLean. *Continuum Fluid Mechanics and the Navier-Stokes Equations*. John Wiley and Sons, 2012.

[6] Nancy Hall. Euler equations. *NASA Glenn Research Center*, 5 2021.

[7] Philip McCord Morse and K Uno Ingard. *Theoretical acoustics*. Princeton University press, 1986.

[8] Britannica The Editors of Encyclopaedia. Eddy. *Encyclopedia Britannica*, 6 2006.

[9] COMSOL Multiphysics. Simulate single-phase and multiphase flow, 2023.

[10] COMSOL Multiphysics 6.0. Flow through a pipe elbow, 2023.

[11] COMSOL Multiphysics. How to build a mesh in comsol mulitphysics, 2023.

[12] Walter Frei. Which turbulence model should i choose for my cfd application?, 7 2017.

[13] Osborne Reynolds. *Papers on Mechanical and Physical Subjects*, volume 3. Cambridge University Press, 1903.

[14] Maurits H. Silvis. *Physics-based turbulence models for large-eddy simulation: Theory and application to rotating turbulent flows*. PhD thesis, University of Groningen, 10 2020.

[15] Robert W. Sterner, Gaston E. Small, and James M. Hood. The conservation of mass. *Nature Education*, 2011.

[16] Ronald L. Panton. *Incompressible Flow*. Hoboken: John Wiley and Sons, 4 edition, 2013.

[17] G.K. Batchelor. *An Introduction to Fluid Dynamics*. Cambridge Mathematical Library series, Cambridge University Press, 2000.

[18] Gregory F. Homicz. Computational fluid dynamic simulation of pipe elbow flow. *SAND Report*, pages 17–18, 8 2004.

[19] Isaac Newton. *Newton's Principia: The mathematical principles of natural philosophy*. Daniel Adee, 1846.

[20] Phillip M. Ligrani. A study of dean vortex development and structure in a curved rectangular channel with aspect ratio of 40 at dean numbers up to 430. *NASA Technical Reports Server*, 7 1994.

[21] L.S. Yao and S.A. Berger. Flow in heated curved pipes. *Annual Review of Fluid Mechanics*, pages 339–354, 1978.

6 Appendix

A Vorticity Contour Plots for One Elbow Systems

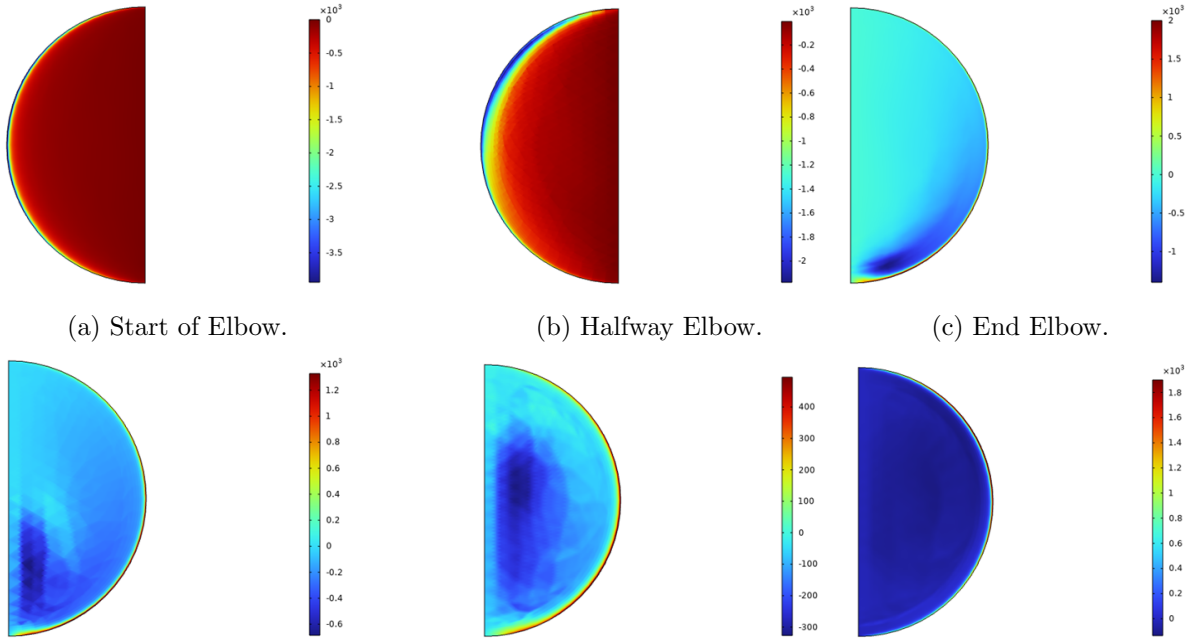

(a) Start of Elbow. (b) Halfway Elbow. (c) End Elbow.

(d) L = 0.1 m. (e) L = 0.2 m. (f) End of System.

Figure A.1: Vorticity contour plots for benchmark model at different stages with colour legend for system with one elbow.

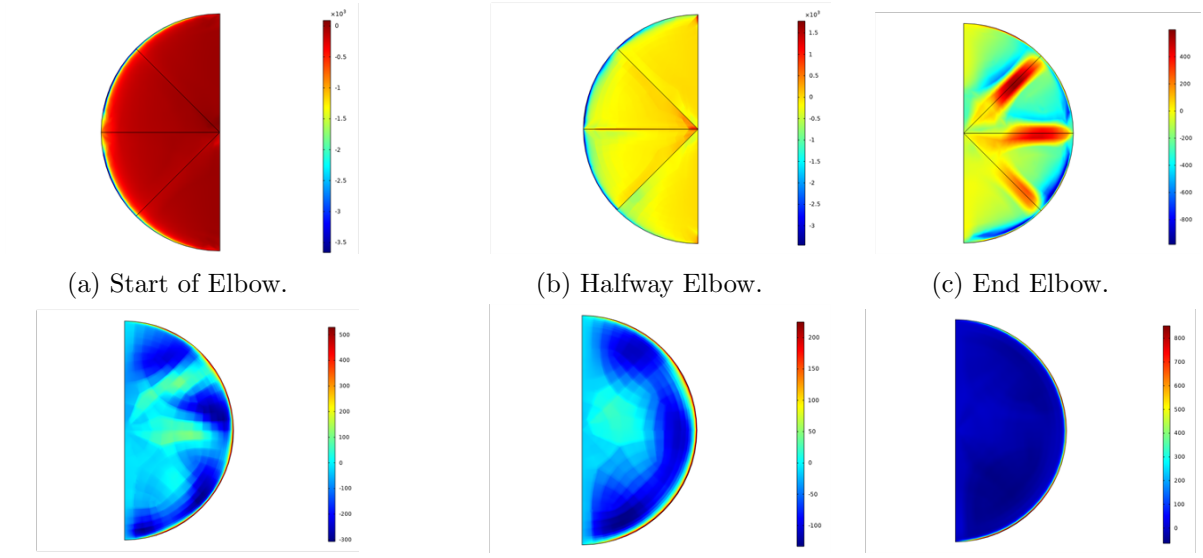

(a) Start of Elbow. (b) Halfway Elbow. (c) End Elbow.

(d) L = 0.1 m. (e) L = 0.2 m. (f) End of System.

Figure A.2: Vorticity contour plots for fin type flow straightener at different stages with colour legend for system with one elbow.

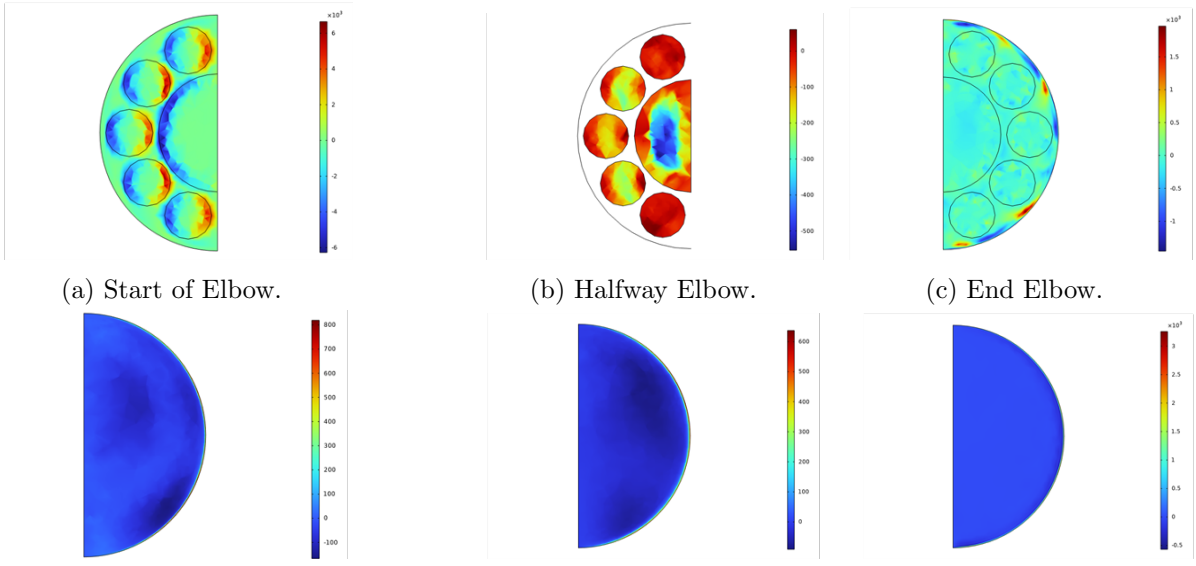

(a) Start of Elbow. (b) Halfway Elbow. (c) End Elbow.

(d) L = 0.1 m. (e) L = 0.2 m. (f) End of System.

Figure A.3: Vorticity contour plots for Disturbance plate A at different stages with colour legend for system with one elbow.

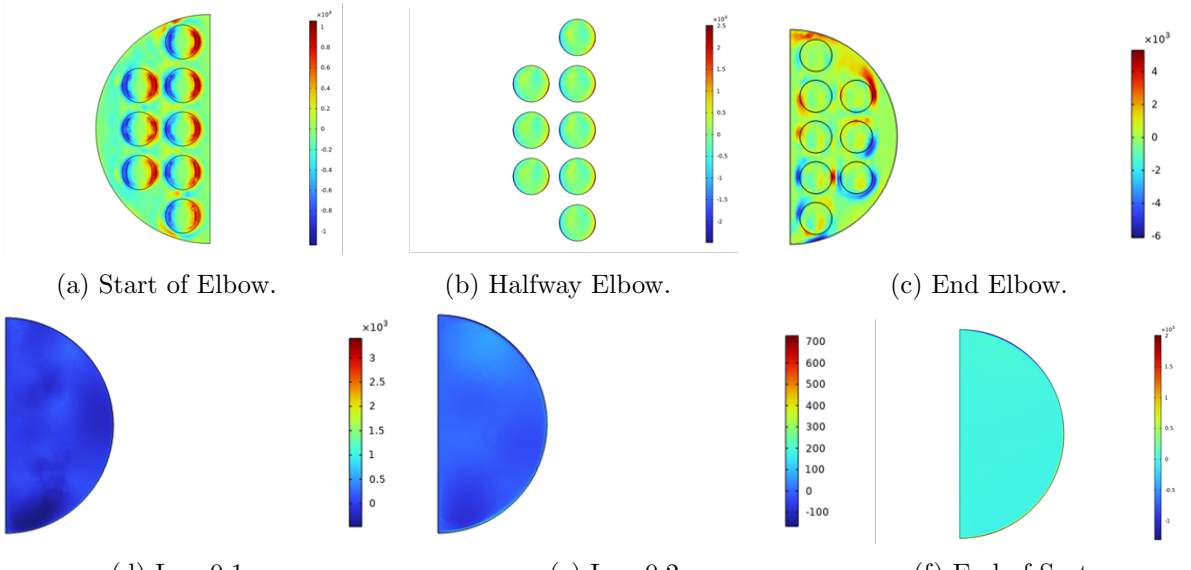

(a) Start of Elbow. (b) Halfway Elbow. (c) End Elbow.

(d) L = 0.1 m. (e) L = 0.2 m. (f) End of System.

Figure A.4: Vorticity contour plots for Disturbance plate B flow straightener at different stages with colour legend for system with one elbow.

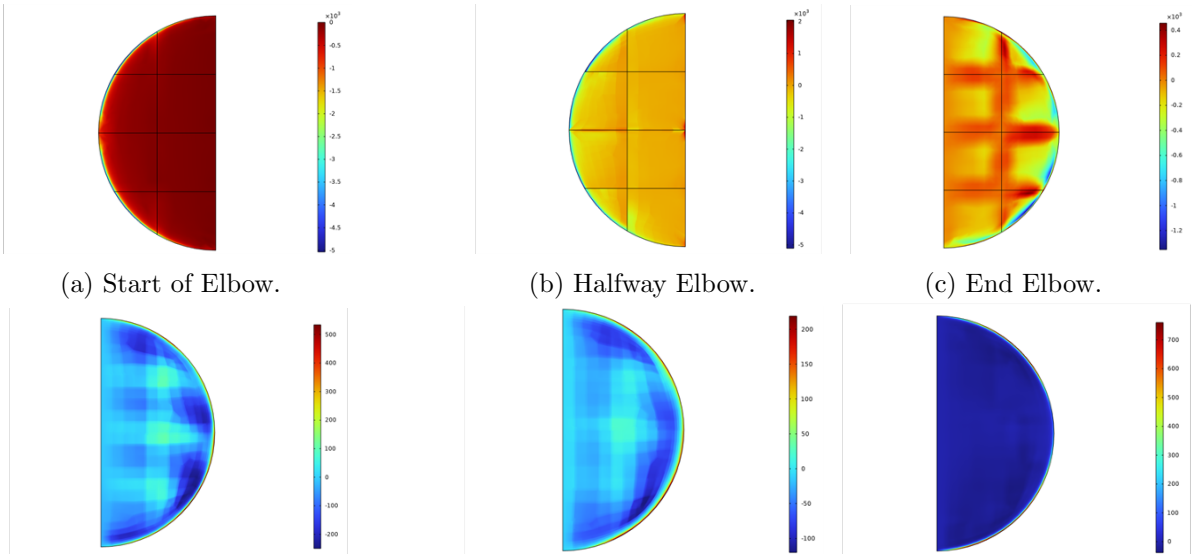

(a) Start of Elbow. (b) Halfway Elbow. (c) End Elbow.

(d) L = 0.1 m. (e) L = 0.2 m. (f) End of System.

Figure A.5: Vorticity contour plots for netting structure flow straightener at different stages with colour legend for system with one elbow.

B Vorticity Contour Plots for Two Elbows In-Plane Systems

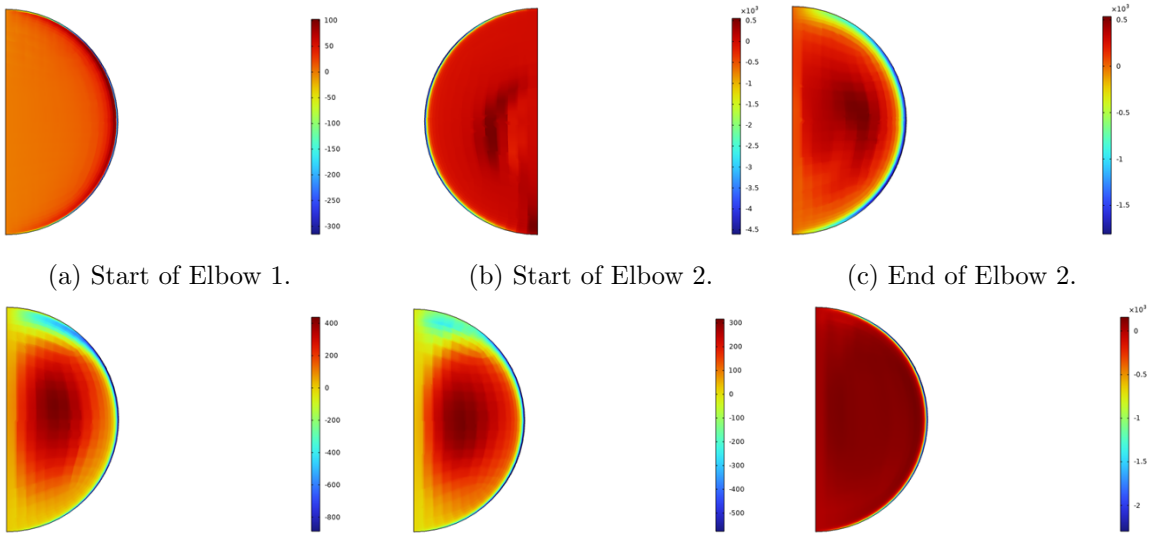

(a) Start of Elbow 1. (b) Start of Elbow 2. (c) End of Elbow 2.

(d) L = 0.1 m. (e) L = 0.2 m. (f) End of System.

Figure A.6: Vorticity contour plots for benchmark model at different stages with colour legend for system with two elbows in-plane.

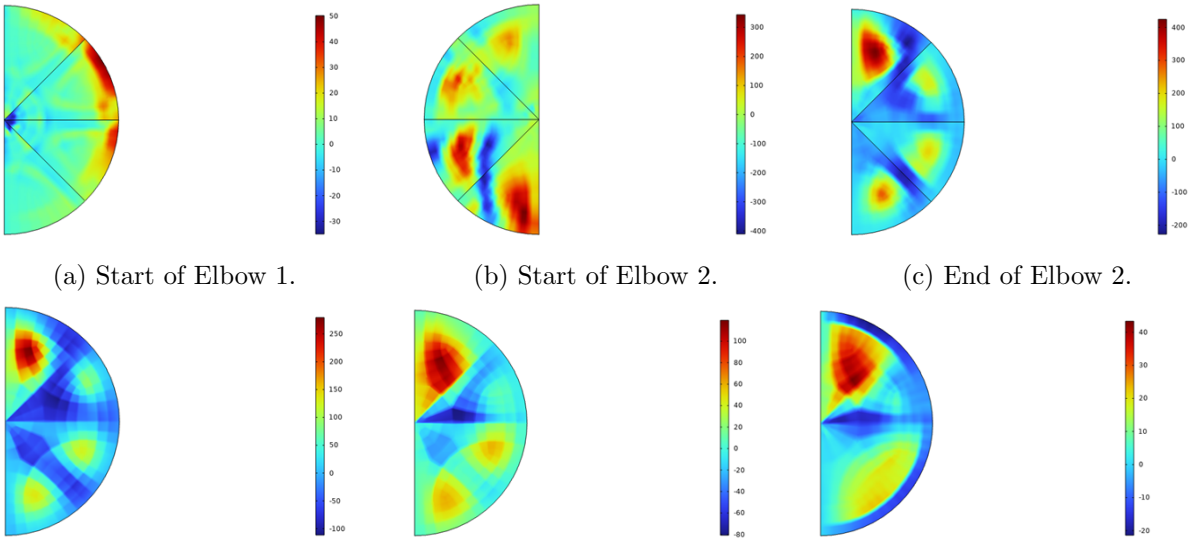

(a) Start of Elbow 1. (b) Start of Elbow 2. (c) End of Elbow 2.

(d) L = 0.1 m. (e) L = 0.2 m. (f) End of System.

Figure A.7: Vorticity contour plots for fin type flow straightener at different stages with colour legend for system with two elbows in-plane.

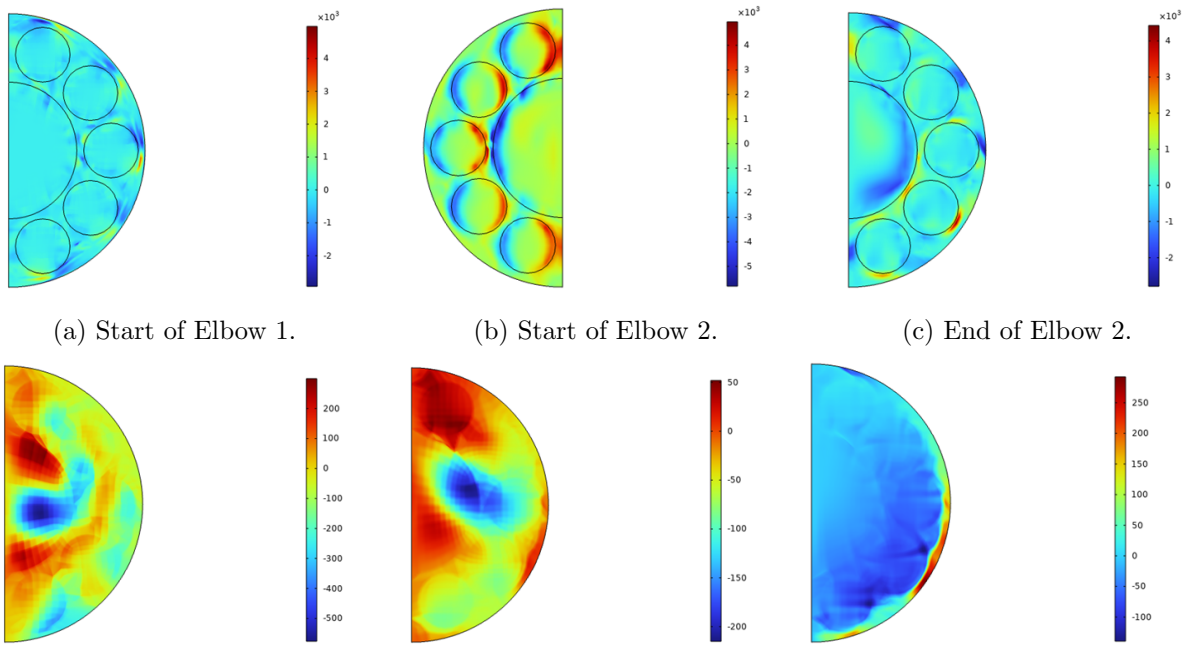

(a) Start of Elbow 1. (b) Start of Elbow 2. (c) End of Elbow 2.

(d) L = 0.1 m. (e) L = 0.2 m. (f) End of System.

Figure A.8: Vorticity contour plots for Disturbance plate A flow straightener at different stages with colour legend for system with two elbows in-plane.

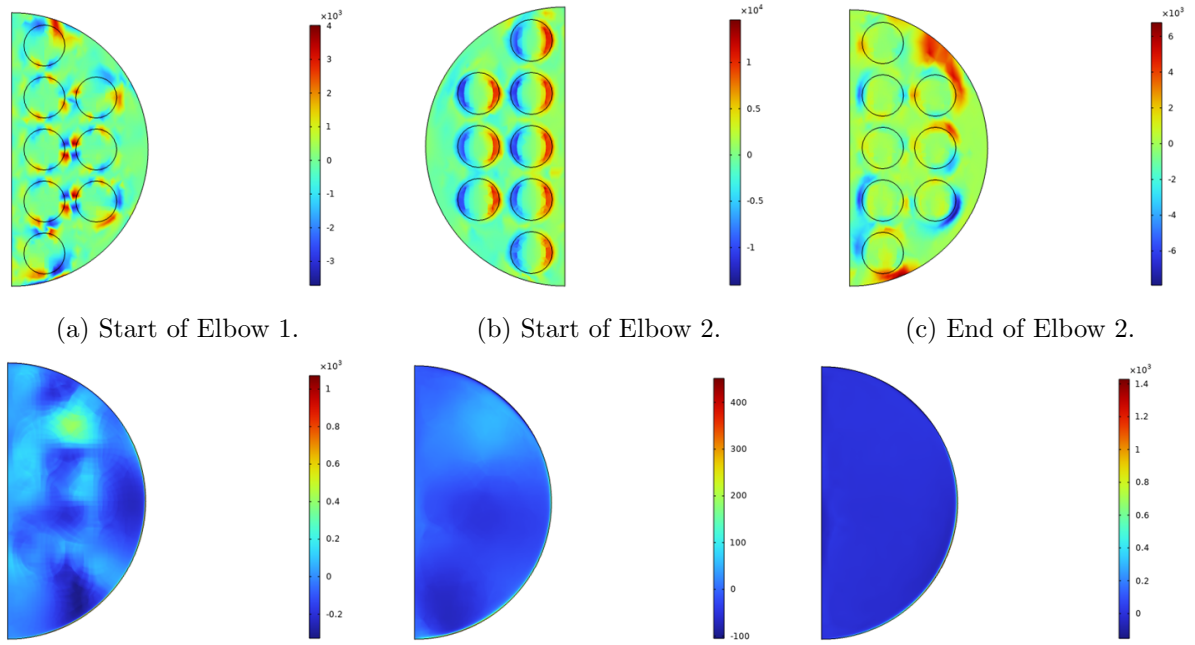

(a) Start of Elbow 1. (b) Start of Elbow 2. (c) End of Elbow 2.

(d) L = 0.1 m. (e) L = 0.2 m. (f) End of System.

Figure A.9: Vorticity contour plots for Disturbance plate B flow straightener at different stages with colour legend for system with two elbows in-plane.

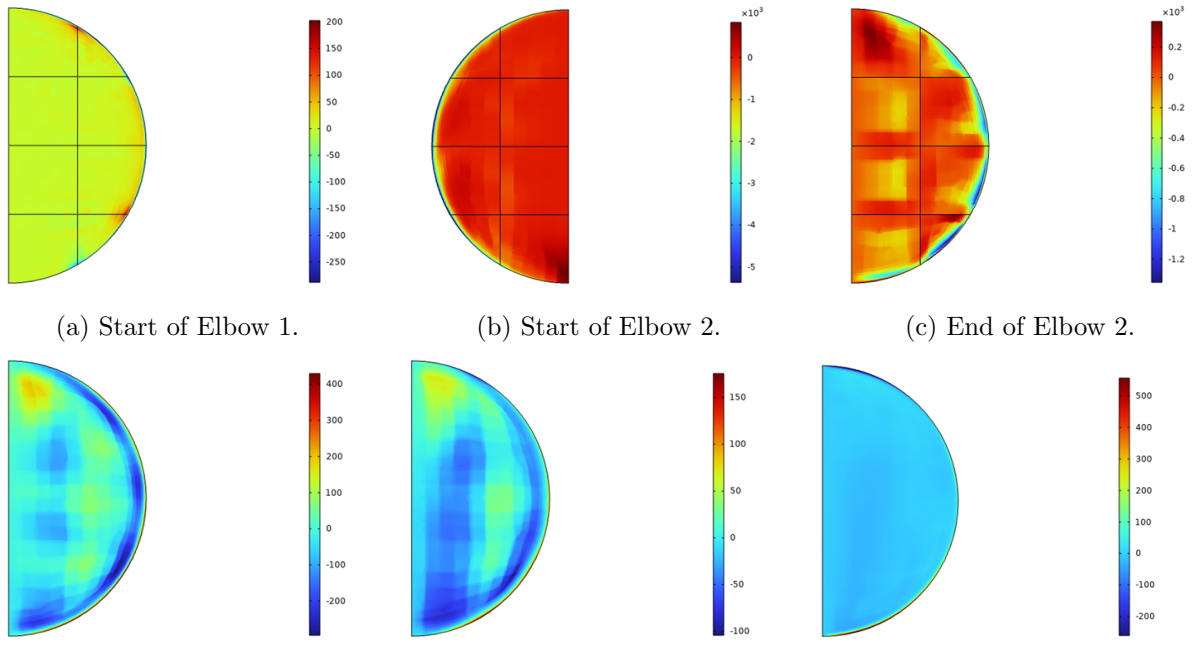

(a) Start of Elbow 1. (b) Start of Elbow 2. (c) End of Elbow 2.

(d) L = 0.1 m. (e) L = 0.2 m. (f) End of System.

Figure A.10: Vorticity contour plots for netting structure flow straightener at different stages with colour legend for system with two elbows in-plane.

C Vorticity Contour Plots for Two Elbows Out of Plane Systems

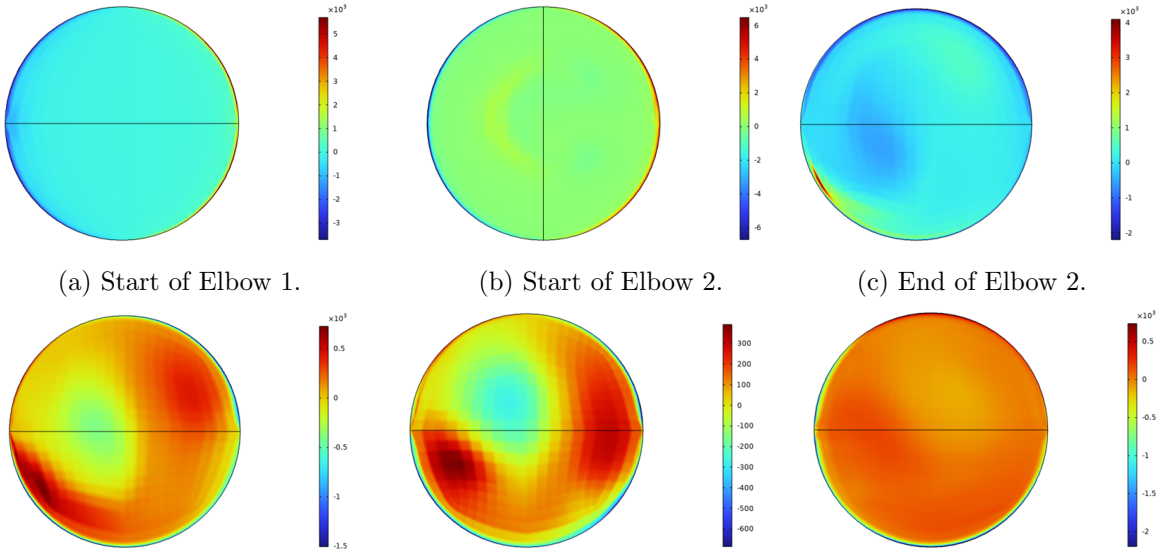

(a) Start of Elbow 1. (b) Start of Elbow 2. (c) End of Elbow 2.

(d) L = 0.1 m. (e) L = 0.2 m. (f) End of System.

Figure A.11: Vorticity contour plots for benchmark model at different stages with colour legend for system with two elbows out of plane.

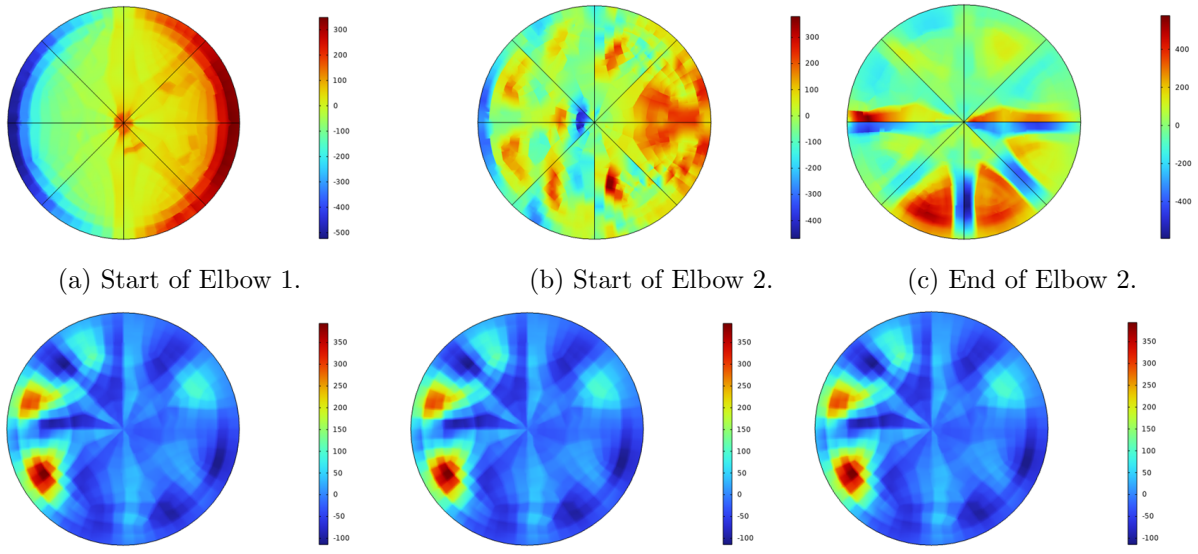

(a) Start of Elbow 1. (b) Start of Elbow 2. (c) End of Elbow 2.

(d) L = 0.1 m. (e) L = 0.2 m. (f) End of System.

Figure A.12: Vorticity contour plots for fin type flow straightener at different stages with colour legend for system with two elbows out of plane.

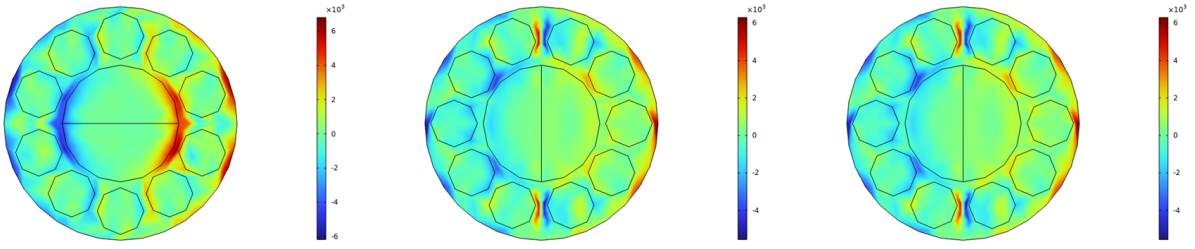

(a) Start of Elbow 1. (b) Start of Elbow 2. (c) End of Elbow 2.

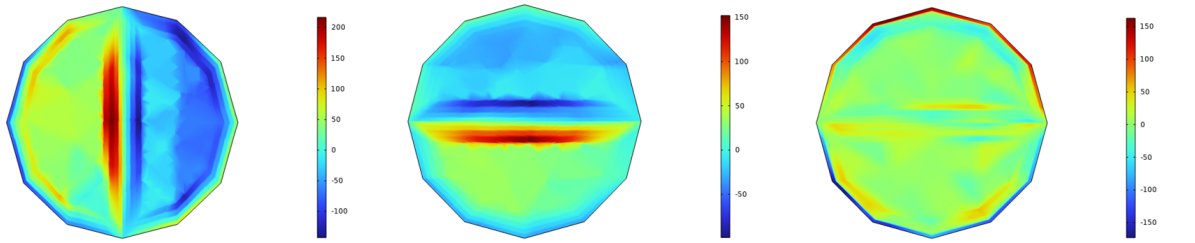

(d) L = 0.1 m. (e) L = 0.2 m. (f) End of System.

Figure A.13: Vorticity contour plots for Disturbance plate A flow straightener at different stages with colour legend for system with two elbows out of plane.

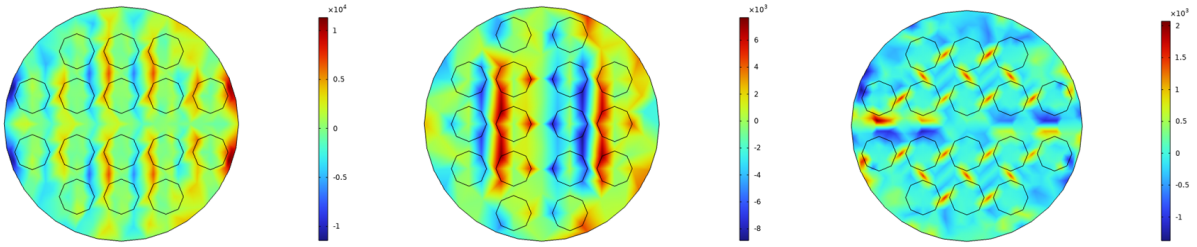

(a) Start of Elbow 1. (b) Start of Elbow 2. (c) End of Elbow 2.

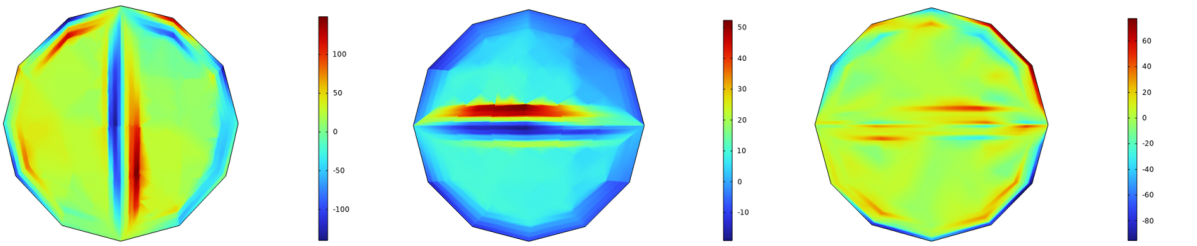

(d) L = 0.1 m. (e) L = 0.2 m. (f) End of System.

Figure A.14: Vorticity contour plots for Disturbance plate B flow straightener at different stages with colour legend for system with two elbows out of plane.

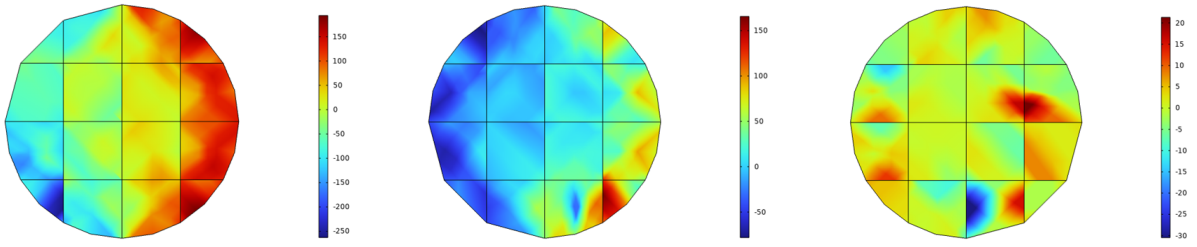

(a) Start of Elbow 1. (b) Start of Elbow 2. (c) End of Elbow 2.

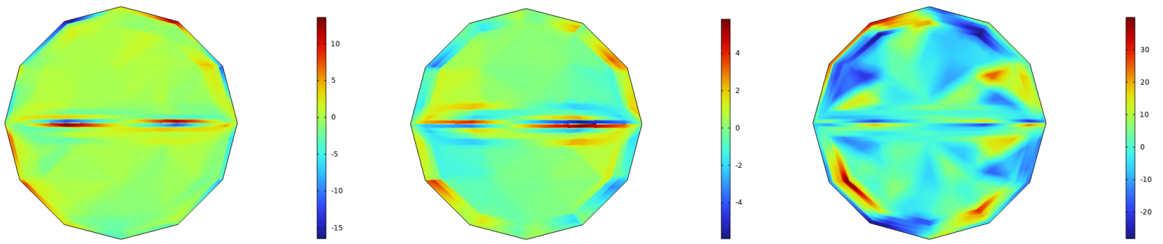

(d) L = 0.1 m. (e) L = 0.2 m. (f) End of System.

Figure A.15: Vorticity contour plots for netting structure flow straightener at different stages with colour legend for system with two elbows out of plane.

D Pressure Distribution

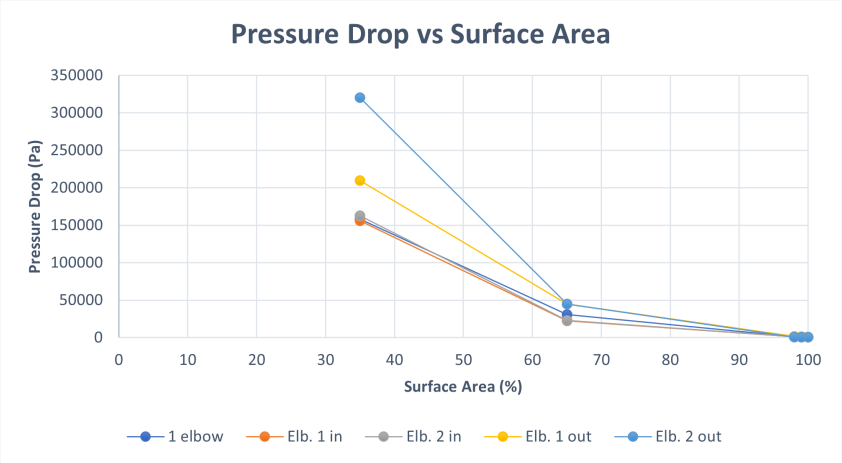

Figure A.16: Pressure drop plotted against the relative surface area.

Table 4: Pressure Drop vs Surface Area.

Surface Area (%)	One Elbow	Elbow 1 in-plane	Elbow 2 in-plane	Elbow 1 out of plane	Elbow 2 out of plane
100	842.8	808.6	517.6	820.4	465.5
100	1035.5	748.9	657.5	1076.3	905.2
65	30885	22708	23271	44555	44952
35	158287	156123	162578	209750	320182
100	1244	1118	980.5	1821	878.8